GENERAL ATOMIC

DIVISION OF

GENERAL DYNAMICS

JOHN JAY HOPKINS LABORATORY FOR PURE AND APPLIED SCIENCE

P.O. BOX 608, SAN DIEGO, CALIFORNIA 92112

GACD-7080
(3-31-66)

Copy No. 4

ELECTRON SHIELDING STUDIES

Technical Progress Report for the Period November 1, 1965 through March 31, 1966

Work done by:

C. Jupiter
R. Scalettar
G. Merkel
W. Hunter

Report written by:

C. Jupiter
R. Scalettar
G. Merkel

During the period of this report the following "reportable items," as defined by Article XII "Reporting of New Technology," evolved:

NONE

Project 447.
NASA, George C. Marshall Space Flight Center
Huntsville, Alabama
Contract Number NAS 8-11304

April 8, 1966

INTRODUCTION

This technical progress report describes the experimental and theoretical work being performed on electron shielding studies under Contract NAS-8-11304 for the George C. Marshall Space Center in Huntsville, Alabama.

The report requirements for this contract were changed by a Contract Amendment dated December 8, 1965. Therefore, this first report under the Amendment covers a five-month (Nov. 1, 1965 - March 31, 1966) period and subsequent reports will cover calendar quarters.

EXPERIMENTAL PROGRAM

1. SUMMARY

A Ce^{137} source was used to check the energy calibration of the 45-degree analyzing magnet.

A number of thick target bremsstrahlung spectra have been obtained for incident electron energies of 10, 8, and 4 MeV electrons.

Inflight positron annihilation spectra were produced by bombarding a thin Be target foil with 6, 8, and 10 MeV positrons. The annihilation spectra were used to determine the response function of the 5 in. by 6 in. NaI(Tl) scintillation spectrometer at 6, 8, and 10 MeV.

The original experimental apparatus has been disassembled. The new scattering chamber has been completed, and vacuum tested. The scattering chamber is now being aligned with the Linac beam tube system.

2. STRIP-SEALED CONTINUOUS ROTATION SCATTERING CHAMBER

A considerable portion of the electron shielding effort during this reporting period has been directed toward the assembly and installation of the new scattering chamber. Photographs of the chamber and associated equipment taken while the chamber was in the process of being aligned with the Linac beam tube system are shown in Figs. 1 to 3.

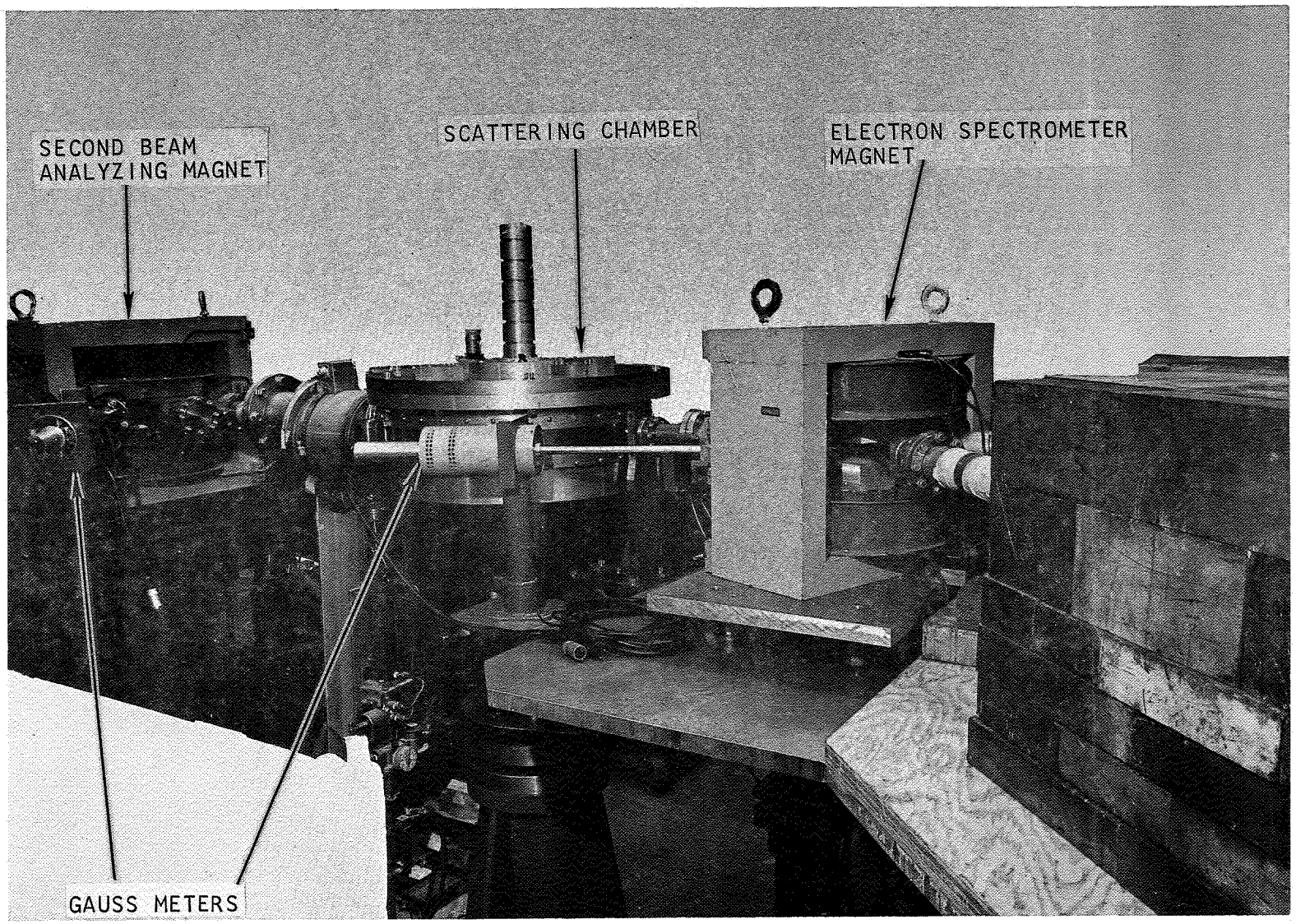

Fig. 1--Scattering chamber and associated equipment - side view

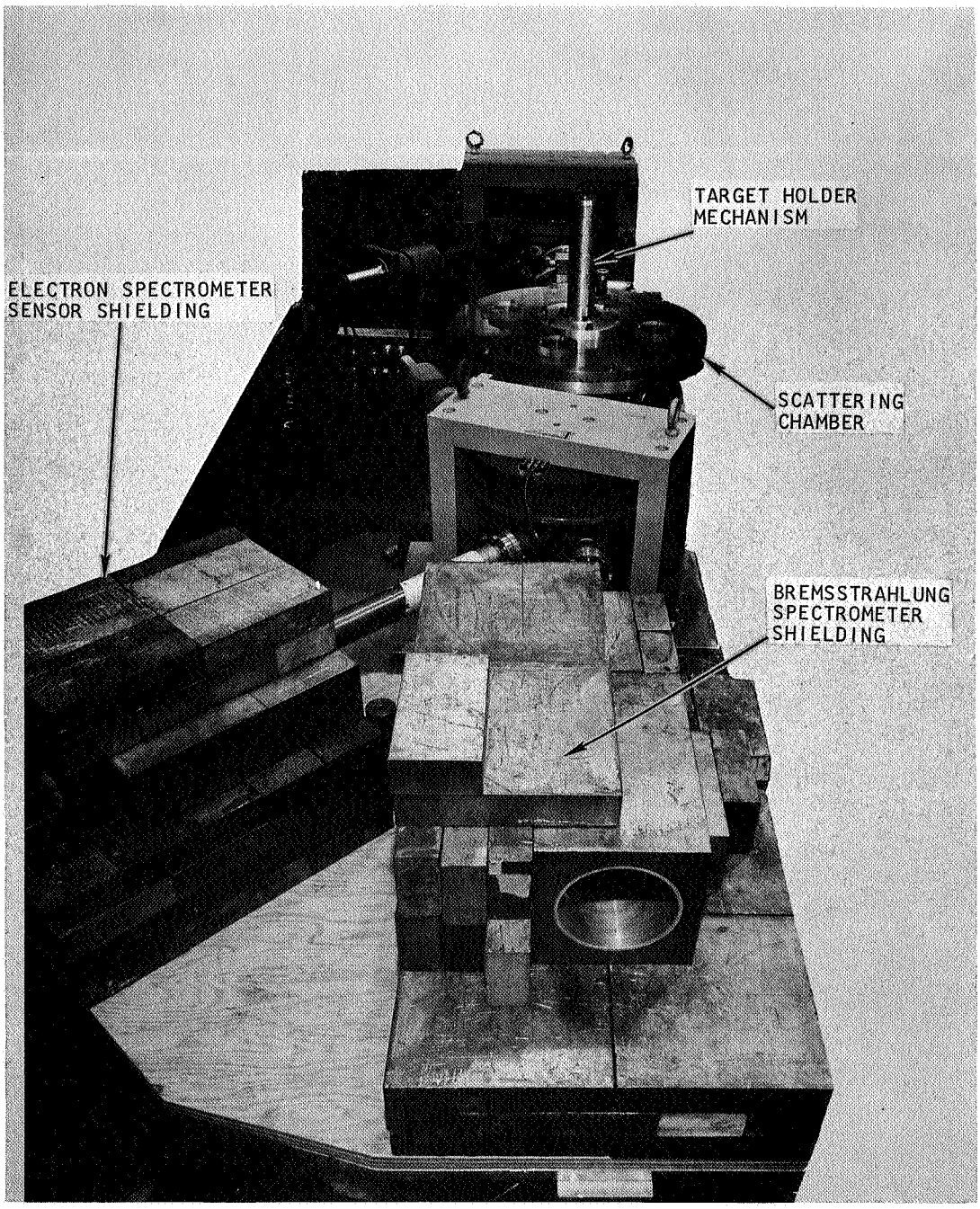

Fig. 2--Scattering chamber and associated equipment - rear view

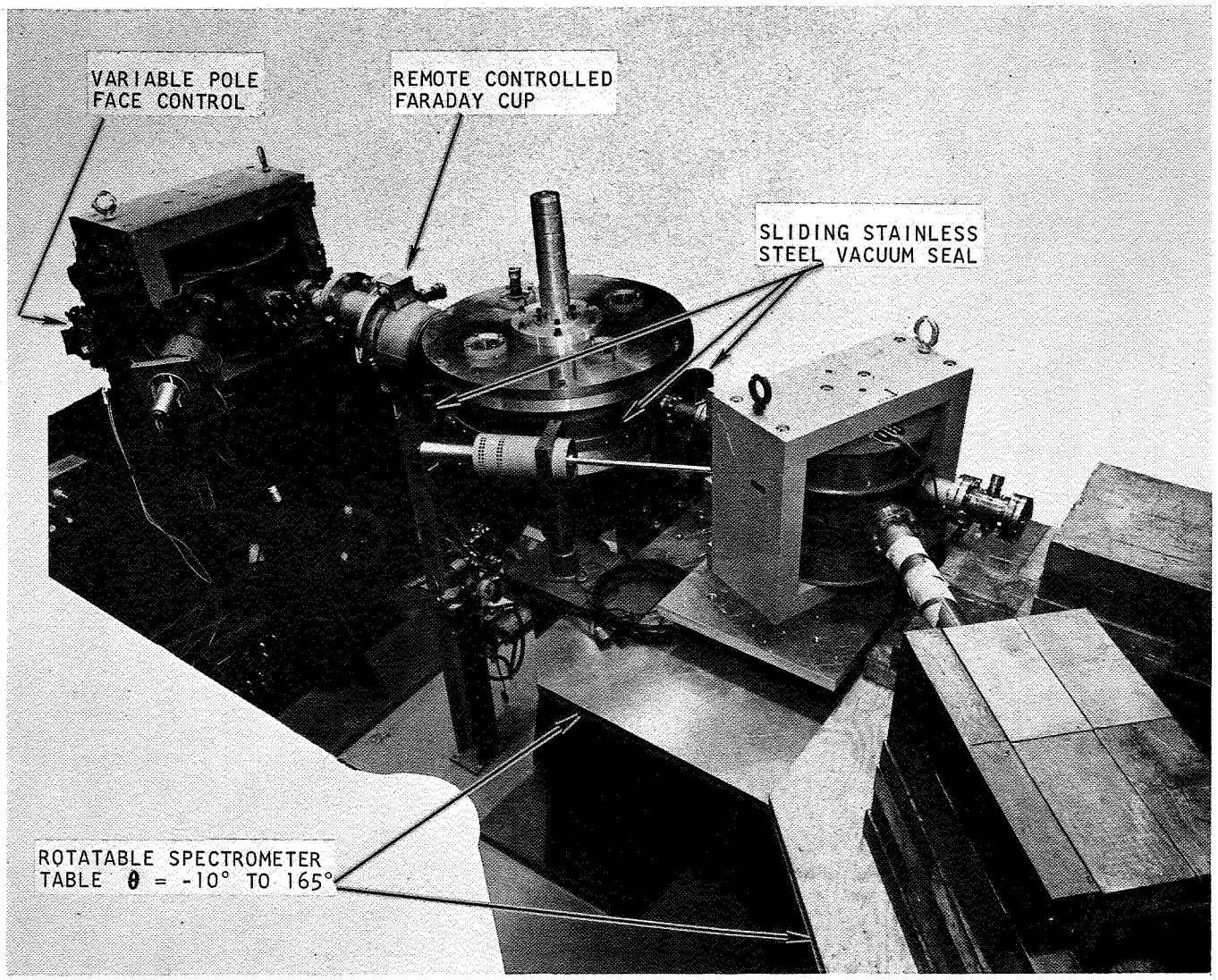

Fig. 3--Scattering chamber and associated equipment - top view

The sliding strip seal is designed so that thin and thick target bremsstrahlung and electron spectrum measurements can be made from 0 degree to 165 degrees. A number of thick target electron transmission measurements, made with the original bellows scattering chamber, are described in the previous Experimental Electron Shielding Studies Report (GACD-6844). One of the first projects involving the new scattering chamber will be the normalization of these relative measurements to absolute values.

3. REDUCTION OF ENERGY ANALYZING SLIT WIDTH

A schematic diagram of the beam translation and analyzing system is shown in Fig. 4. The beam analyzing slit width W has been reduced from 1/8 in to 1/16 in. With the variable pole face direction β_1 perpendicular to the line XX the energy resolution of the beam after passing through the matched pair of magnets is given by

$$\frac{\Delta p}{p} = \frac{W}{S} \text{ or } \frac{\Delta E}{E} \simeq \frac{W}{S} \text{ for } E \gg M_o C^2$$

The reduction in the beam analyzing slit width should therefore result in an improvement in beam resolution from 2% to 0.5%. This is particularly desirable for the measurement of electron scattering in thin targets.

4. BREMSSTRAHLUNG SPECTRA MEASUREMENTS

Prior to dismantling the bellows scattering chamber it was used to obtain a number of thick target bremsstrahlung spectra for 10, 8, and 4 MeV incident electrons. Typical experimental results for 10 MeV electrons incident upon a 0.8 range Al target are shown in Figs. 5 and 6. The histograms shown in Figs. 5 and 6 are the results of Berger's Monte Carlo calculations for 10 MeV electrons incident on 0.8 range targets. Since the data have not yet been corrected for the effects of the NaI(Tl) response functions, the comparisons between experiment and calculation are very qualitative and are only intended to show general trends.

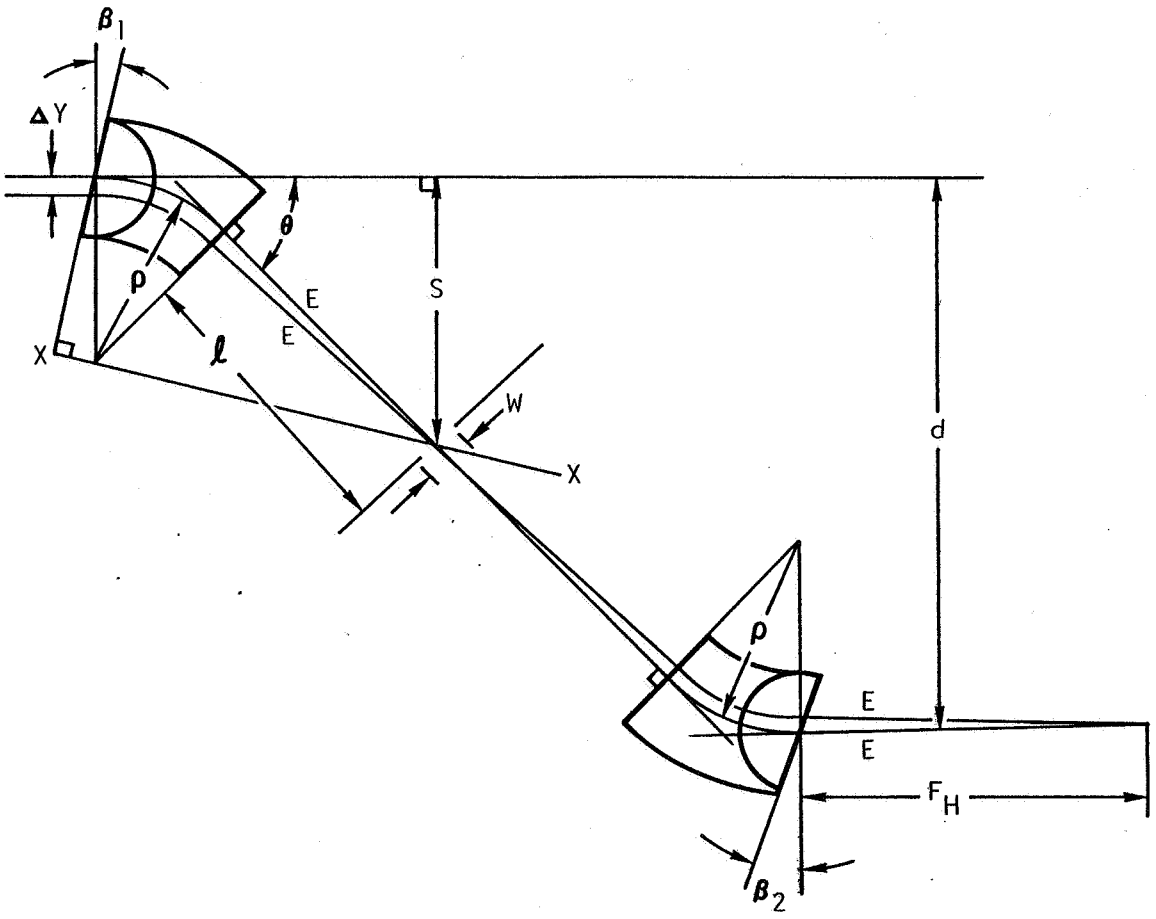

Fig. 4--Diagram of matched pair of beam analyzing and translation magnets

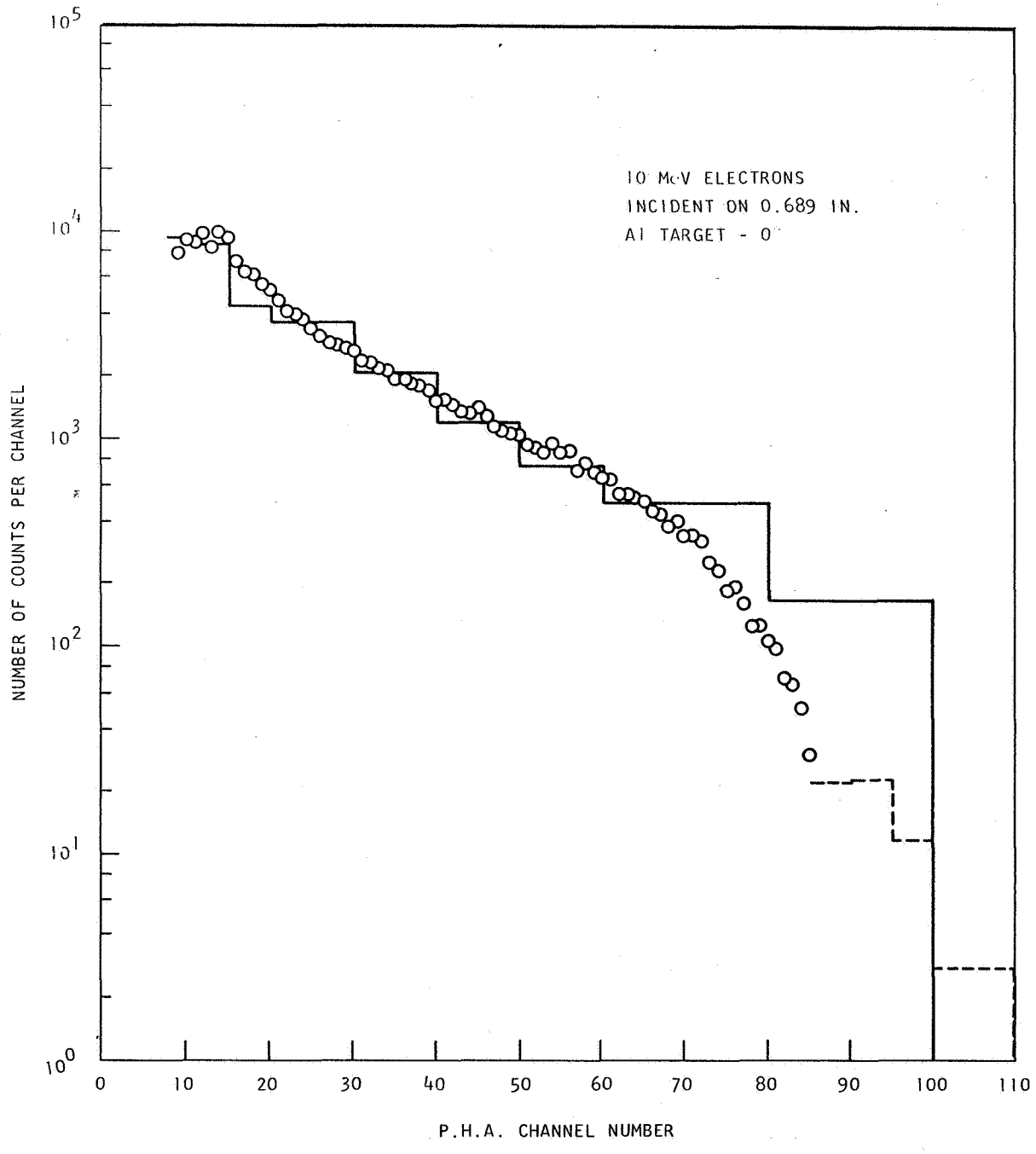

Fig. 5--Bremsstrahlung spectrum at 0 degree - the histogram corresponds to Berger's Monte Carlo calculations

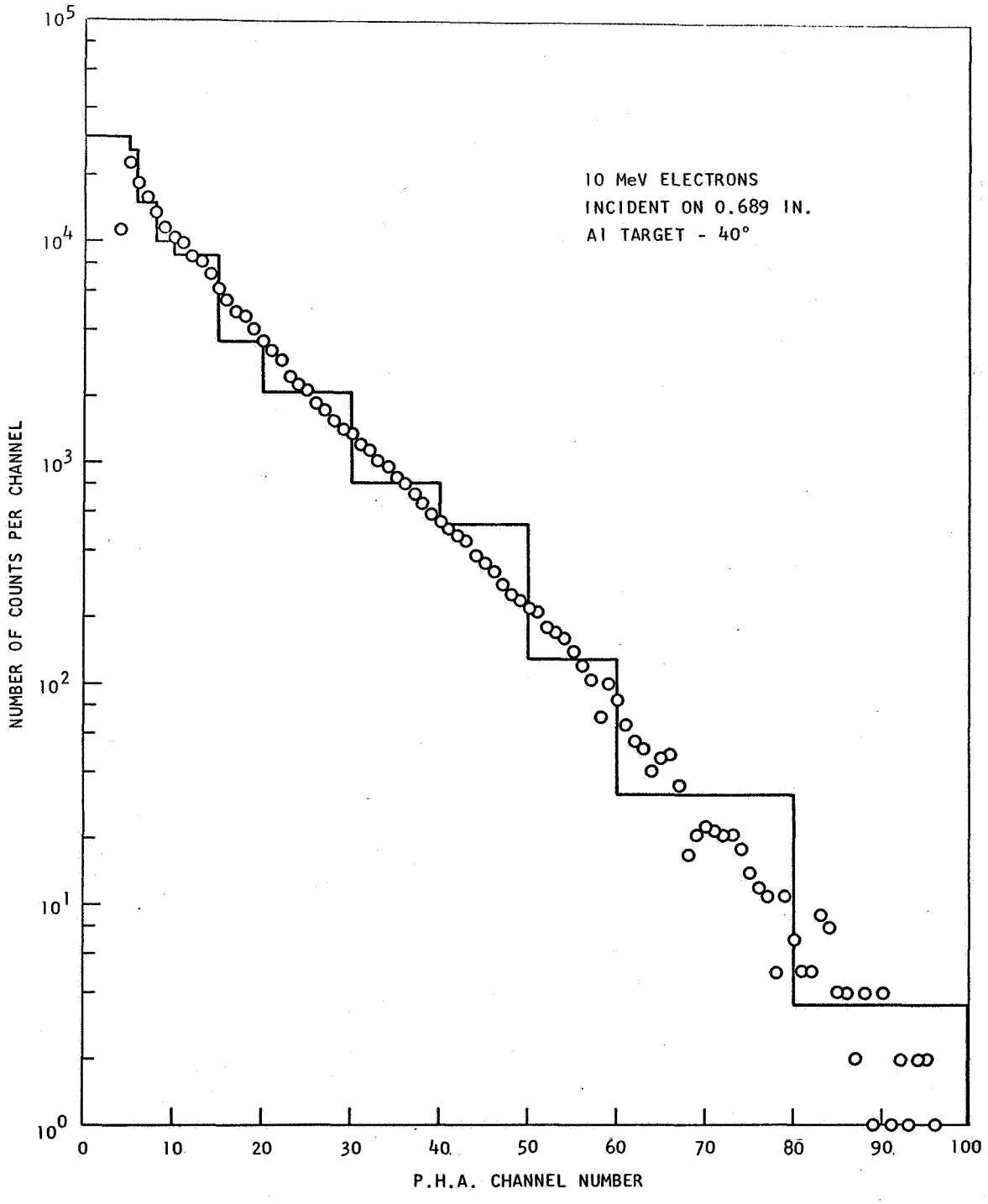

Fig. 6--Bremsstrahlung spectrum at 40 degrees - the histogram corresponds to Berger's Monte Carlo calculations

5. Ce^{137} SOURCE CALIBRATION

A 20-millicurie Ce^{137} internal conversion source was used to check the calibration of the electron spectrometer. The calibration check, made immediately before the bellows scattering chamber was dismantled, agreed to within 1% of the ion source calibration described in our report GACD-6844. The spectrum of the internal K conversion line as a function of electron spectrometer magnetic field strength is shown in Fig. 7. Figure 8 shows the response function of the electron spectrometer NaI(Tl) crystal sensor to the analyzed 0.624 MeV internal conversion electrons. The low energy tail of the response function shown in Fig. 6 is the result of electrons backscattering from the NaI(Tl) scintillation counter. Since the albedo of electrons is appreciably smaller for anthracene than for NaI(Tl), the magnitude of the tail can be greatly decreased by the use of an anthracene crystal in place of the NaI(Tl) crystal.

The 5% FWHM of the electron spectrum shown in Fig. 5 is due to the absorption of electrons in the relatively thick Ce^{137} source and is not a measure of the resolving power of the electron spectrometer.

6. PILE-UP CORRECTIONS

If the true pulse height distribution for photons of energy E is given by N(E) then the measured spectrum, $N_m(E)$, which includes pulse pileup is given by

$$N_m(E) = N(E)(1-2p) + p \frac{\int_0^E N(E)\, N(E-E')\, dE}{\int_0^{Emax} N(E')\, dE'} \qquad (1)$$

where p is the probability during a spectrum experiment of recording two photons. Equation (1) can be rearranged to yield

$$N(E) = N_m(E) + 2p\,N(E) - p\,\frac{\int_0^E N(E)\,N(E-E')\,dE'}{\int_0^{Emax} N(E')\,dE'} \qquad (2)$$

The probability p is small and N(E) is approximately equal to $N_m(E)$ therefore

$$N(E) \cong N_m(E)\,(1 + 2p) - p\,\frac{\int_0^E N_m(E)\,N_m(E-E')\,dE'}{\int_0^{Emax} N_m(E')\,dE'} \qquad (3)$$

In practice N(E) can be calculated by successively applying Eq. (2). The value arrived at can then be checked with Eq. (1). This technique has been used to correct the bremsstrahlung and positron annihilation gamma spectra measured here. It has the advantage of allowing data to be taken at a faster rate than otherwise possible; in this way, LINAC usage is reduced, and data pulses are collected at a much higher rate than the background pulser. Distortion in the spectrum due to pulse pileup accompanying the high data collection rate is removed by the analytical method described above.

7. RESPONSE FUNCTION MATRIX AND MATRIX INVERSION

The experimental 28 by 28 Response Function Matrix obtained by J. H. Hubbell[1] for a 4-in. long by 5-in. diameter NaI(Tl) crystal spectrometer for energies up to 8 MeV has been modified to be applicable to a 6-in. long by 5-in. diameter NaI(Tl) crystal spectrometer. The modification included correcting the crystal efficiency as a function of photon energy for the larger crystal and an extension of the energy range by the addition of three energy bins having widths proportional to $\sqrt{E}$ - allowing an extension up to 13 MeV.

[1] J. H. Hubbell, "Response of a Large NaI Detector to High Energy X-Rays", Rev. Sci. Instr. 29, 65, (1958).

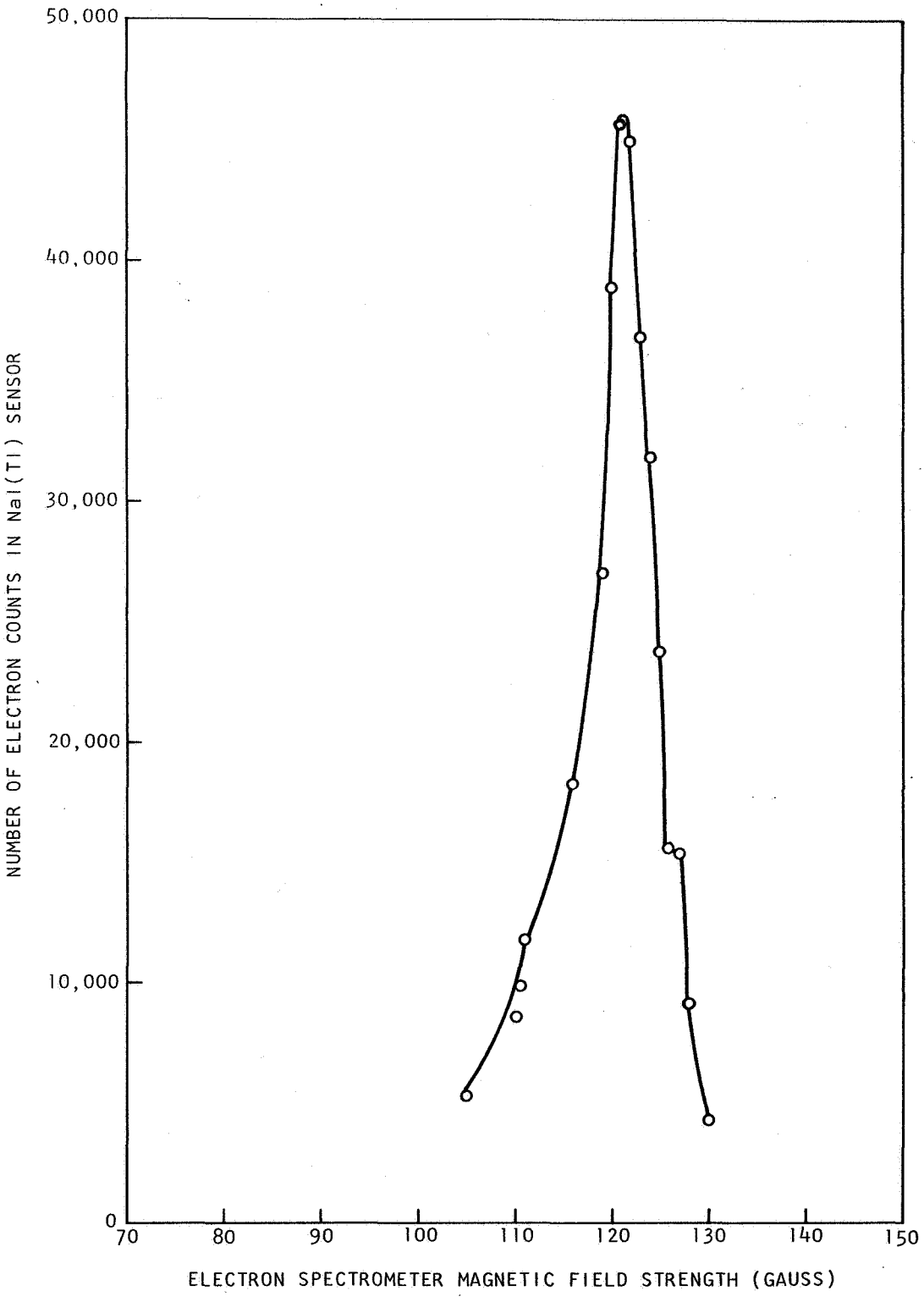

Fig. 7--Spectrum of the internal K conversion line of a Ce^{137} source as a function of electron spectrometer magnetic field strength

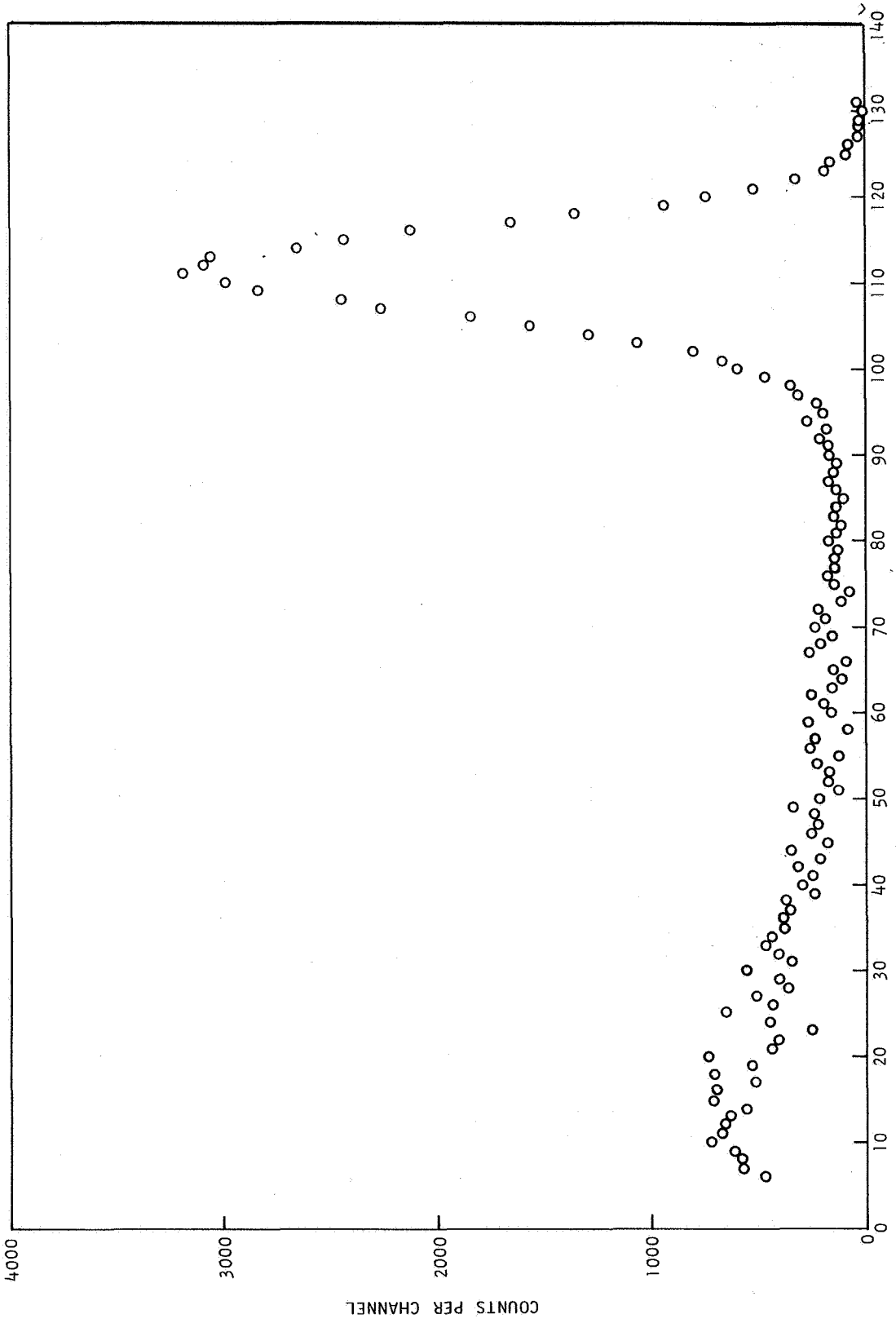

Fig. 8--Pulse height response of NaI(Tℓ) electron detector to magnetically analyzed 624.33 keV internal conversion electrons from Cs^{137} source

Experimental inflight positron annihilation spectra obtained at 6, 8, and 10 MeV have been used to check the modifications and also to extend Hubbell's response function matrix to a 35 by 35 matrix that covers energies up to 11 MeV. The matrix has been inverted, and the response function corrections are now being applied to the experimental 10, 8, and 4 MeV bremsstrahlung spectra.

Electron Shielding Quarterly Report - Theoretical

We shall herein describe certain of the advances made during this period in the theoretical analysis of the electron transport problem.

(a) With regard to the Bethe eigenfunction solution, we have previously shown that the electron distribution in position, x, energy, E, and angle cosine, μ, is given by

$$f(x,E,\mu) = a(x,E) + b(x,E)\mu + \sum_{n=-\infty}^{+\infty} C_n(x,E)\psi_n(\mu) \qquad (1)$$

where the rapid convergence of this series solution is ensured for beam geometry, by the large magnitude of the eigenvalues, k_n, of the Bethe eigenfunctions $\psi_n(\mu)$. The first pair of eigenvalues is determined numerically to be

$$k_1 = +14.559, \; k_{-1} = -14.559 \qquad (2)$$

and the associated eigenfunctions are

$$\psi_{\pm 1}(\mu) = a_o\left\{1 - \frac{k_{\pm 1}}{2}(1-\mu) + \frac{k_{\pm 1}^2}{16}(1-\mu)^2 \ldots\right\} \qquad (3)$$

and have been computed numerically. The direct evaluation of higher eigenvalues from the determinantal or continued fraction equation is

cumbersome.

Therefore a generalized W.K.B. method has been developed following Dorodnitsyn. Our problem, involving as it does two singular points at $\mu = \pm 1$ and a turning point at $\mu = 0$, is more complicated than the cases treated by Dorodnitsyn but the essential idea is the same. The solution of the Bethe equation regular at $\mu = 1$ is

$$\psi(\mu) = \frac{1}{\sqrt{1-\mu}}\, e^{-1/2\int_0^{1-\mu}\left[\frac{2(1-x')}{2-x'} - 1\right]dx'}\, Z_1(\mu-1;1) \tag{4}$$

where

$$Z_1(x;1) = \frac{V_1(k\omega(x);1)}{\sqrt{\omega'(x)}} \tag{5}$$

and

$$\omega(x) = \left[1/2\int_0^{x}\sqrt{\frac{1-x'}{x'(2-x')}}\,dx'\right]^2 \tag{6}$$

and V_1 is tabulated in Smirnov's "Airy Functions". A similar form with $1 - \mu$ replaced by $1 + \mu$ holds for the solution regular at $\mu = -1$. Continuity of the logarithmic derivatives (vanishing of the Wronskian⟷

linear dependence) through the turning point at $\mu = 0$ yields

$$k_n = \pm (n + 1/4)^2 \pi^2 \qquad (7)$$

and the associated eigenvalues of the form (4). We find that the expansion coefficients fall of as $k_n^{-3/4}$ even near the boundaries and exhibit a rapid approximately exponential decay away from the boundaries. The details of the analysis for the $C_n(x,E)$ have been previously exhibited and the result for $f(x,E,\mu)$, as indicated in the figures, show quite satisfactory agreement with the unnormalized experimental energy straggling and angular distribution data.

(b) With regard to the relativistic inelastic electron cross sections required is the DSN calculation, a combination of the Bethe and Watson-Goldberger arguments leads to a relativistic form factor

$$|a_o|^2 S(q) + (a_o \vec{a}^* + a_o^* \vec{a}) \cdot \left(\sum_\gamma \frac{\vec{v}_\gamma}{c} \right)_{oo}$$

$$+ \sum_\gamma \left[(\vec{a} \cdot \frac{\vec{v}_\gamma}{c})(\vec{a}^* \cdot \frac{\vec{v}_\gamma}{c}) \right]_{oo}$$

$$+ 2 \, \mathrm{Re} a_o^* \vec{a} \cdot \left\{ \sum_{\gamma \neq K} \left(\frac{\vec{v}_\gamma}{c} e^{i\vec{q}\cdot(\vec{r}_\gamma - \vec{r}_K)} \right)_{oo} \right. \qquad (8)$$

$$-\sum_{\gamma,K} (e^{-i\vec{q}.\vec{r}_\gamma})_{oo} (\vec{\underset{c}{v}}_\gamma e^{i\vec{q}.\vec{r}_K})_{oo} \Bigg\}$$

$$-\sum_{\gamma \neq K} \left[(\vec{a}^* . \vec{\underset{c}{v}}_\gamma)(\vec{a}^* . \vec{\underset{c}{v}}_K) e^{i\vec{q}.(\vec{r}_\gamma - r_K)} \right]_{oo}$$

$$-\left| \sum_{\gamma} (\vec{a} \cdot \vec{\underset{c}{v}}_\gamma e^{i\vec{q}.\vec{r}_\gamma})_{oo} \right|^2$$

Here S(q) is the analogue of the non-relativistic Morsefunction, $\vec{v}_\gamma$ and $\vec{r}_\gamma$ and are velocities and positions of the γth atomic electron, $\vec{q} = \vec{p}' - \vec{p}$ is the momentum transfer of the incident electron and

$$a_o = s(\vec{p}) s^*(\vec{p}'); \quad \vec{a} = -(s^*(\vec{p}')\vec{\alpha} s(\vec{p}))$$

where s is the spinor of the incident (or scattered) electron. A generalization of the relativistic Thomas-Fermi model due to Gilvarry is used for the numerical evaluation of the matrix elements occurring in (8).

(c) The computation of the bremsstrahlung cross sections and the corrections to the electron-photon transport equations, following the method of Watson, are being carried out in the radiation gauge of

$$-\sum_{\gamma,\kappa}\left(e^{-i\vec{q}\cdot\vec{r}_\gamma}\right)_{oo}\left(\frac{\vec{v}_\gamma}{c}e^{i\vec{q}\cdot\vec{r}_\kappa}\right)_{oo}\Bigg\}$$

$$-\sum_{\gamma\neq\kappa}\left[\left(\vec{a}^{\,*}\cdot\frac{\vec{v}_\gamma}{c}\right)\left(\vec{a}^{\,*}\cdot\frac{\vec{v}_\kappa}{c}\right)e^{i\vec{q}\cdot(\vec{r}_\gamma-\vec{r}_\kappa)}\right]_{oo}$$

$$-\left|\sum_{\gamma}\left(\vec{a}\cdot\frac{\vec{v}_\gamma}{c}e^{i\vec{q}\cdot\vec{r}_\gamma}\right)_{oo}\right|^2$$

Here $S(q)$ is the analogue of the non-relativistic Morsefunction, $\vec{v}_\gamma$ and $\vec{r}_\gamma$ and are velocities and positions of the γth atomic electron, $\vec{q} = \vec{p}' - \vec{p}$ is the momentum transfer of the incident electron and

$$a_o = s(\vec{p})s^*(\vec{p}'); \quad \vec{a} = -(s^*(\vec{p}')\vec{\alpha}s(\vec{p}))$$

where s is the spinor of the incident (or scattered) electron. A generalization of the relativistic Thomas-Fermi model due to Gilvarry is used for the numerical evaluation of the matrix elements occurring in (8).

(c) The computation of the bremsstrahlung cross sections and the corrections to the electron-photon transport equations, following the method of Watson, are being carried out in the radiation gauge of

Schwinger and Johnson. The details of these and the previous calculations are described in previously submitted reports as all as addenda thereto now in preparation.